Controlling A Meandering Wake: Insights From Full-Information Control

Parul Singh[1] and Peter Seiler[2]

***Abstract*— In this paper we design and analyze a full-information H_∞ controller to in order to reduce the wake meandering behind a wind turbine. The low frequency instability that causes wake meandering can cause unsteady mechanical loads on the downstream turbines resulting in early onset of material fatigue. Controlling the wake meandering in a wind farm can therefore reduce maintenance costs. The control design and analysis in this paper proceeds in two steps. First, a linear reduced order model of the turbine is obtained using snapshots from a higher-order nonlinear 2D actuator-disk model. A full-information H_∞ controller is then designed for the reduced order model assuming access to the entire flow field and disturbance input. The control performance is evaluated by simulations on the higher-order nonlinear model. The full-information controller can not be implemented in practice. However, it can provide insight into control design for wind farms such as identifying desirable locations to measure the downstream flow.**

I. INTRODUCTION

Many states in United States have a regulatory mandate to increase production of energy from renewable sources. Wind energy will be a significant contributor in achieving this target. However, the presence of wake meandering behind turbines in a wind farm can pose a problem in achieving this goal. The meandering wake causes downstream turbines to experience unsteady structural loads which can be damaging and add to the maintenance costs. By controlling this meandering wake therefore, wind energy production can be made more efficient in order to maximize the power of existing wind farms. In this paper we present an ideal, full-information control design to control the wake meandering behind a single turbine. The insights gained from this control design and analysis can be used to design more realistic and implementable controllers for wake control in wind farms.

Wake meandering behind a turbine is characterized as the low-frequency periodic lateral displacement of the wake, generally at downstream distances greater than three times the turbine rotor diameter. It is a well-documented but little understood phenomenon. The exact mechanism causing this meandering instability is not yet known but several theories [1] have been proposed in literature. There is evidence to suggest that the underlying mechanism behind wake meandering is similar to the mechanism behind the instability of helical large-scale coherent structures found behind bluff bodies. For axisymmetric bodies, there is no preferred direction of the meandering. However, the fact that a wind turbine has a specific rotational direction breaks the symmetry which results in a preferred direction of the meandering and at a rather distinct frequency [2]. The frequency of meandering appears to depend upon both the thrust coefficient and the tip-speed ratio of the turbine [3].

The literature [4], [5], [6] on wind turbine wake studies shows that, under both steady uniform inflow and more realistic turbulent inflow conditions, approximations of axial turbines as actuator disks or rotating actuator lines successfully produce the wake-meandering instability. Furthermore, there are studies [7], [8] supporting the assumption that the far wake structure predicted using simplified approximations of the turbine geometry provides a good approximation to the wake arising in realistic turbine geometries. Moreover, the results are in reasonable agreement with wind tunnel measurements. The advantage of using these simplified models is that the complete simulation can be run within minutes on a desktop computer and the generated wake is a reasonable approximation to higher-fidelity models.

In this paper, we use the simplifying approximation of the axial turbine as an actuator disk in 2D flow in order to model the wake meandering for our problem (Section II). This nonlinear simulation has approximately $20,000$ states and cannot be directly used to design a controller. Therefore we obtain a reduced order linear model using the input output reduced order modeling (IOROM) technique from [9] in Section III. The identified linear IOROM preserves the input-output behavior of the nonlinear system and is suitable for control design. We assume access to full state as well as the disturbance input and design a full-information H_∞ controller for this reduced model in Section IV. The controller performance is validated in full-order nonlinear simulations and the results are presented in Section V. While a full-information controller can not be implemented in an actual wind farm, the analysis nonetheless gives some valuable insights which are also presented in Section V. These insights can be used for sensor placement to give relevant measurements directly to a output measurement based controller. Finally, conclusions and possible directions for future work are given in Section VI.

II. PROBLEM FORMULATION

A. Wind Turbine Setup

Consider a horizontal axis wind turbine with a rotor diameter of $1D$ [m] located at an arbitrary location in a rectangular field which spans $20D$ in the streamwise x-direction and $5D$ in spanwise y-direction. The turbine is modeled as an actuator disk with an input axial induction factor a. The axial induction factor is defined as $a := 1 - \frac{u}{U_{in}}$ with u denoting the average horizontal air speed across the rotor plane and U_{in} denoting the average inflow air speed. The power captured from the turbine is given by:

[1]Graduate Student, Department of Aerospace and Engineering Mechanics, University of Minnesota, singh461@umn.edu

[2]Assistant Professor, Department of Aerospace and Engineering Mechanics, University of Minnesota, seile017@umn.edu

$$P = \frac{1}{2}\rho A u^3 C_P(a) \tag{1}$$

where ρ [kg/m^3] is the air density, A [m] is the area swept by the rotor, u [m/s] is the wind speed perpendicular to the rotor plane, and $C_P(a)$ is the non-dimensional power coefficient, which is a function of the axial induction factor [10]:

$$C_P(a) = 4a(1-a)^2 \tag{2}$$

As the wind turbine extracts energy from the incoming wind, a wake is generated behind the turbine. The wake interior is characterized by reduced wind speeds and increased turbulence. In the case of a wind farm, we can have a turbine operating in the wakes of upstream turbines and this can result in overall loss of power production and greater structural loading for the downstream turbines. The reduction in velocity immediately downstream of a turbine is directly related to the momentum extracted from the flow which is determined by the turbine thrust coefficient $C_T(a)$, which is also a function of the axial induction factor [10]:

$$C_T(a) = 4a(1-a) \tag{3}$$

The optimal induction factor that maximizes the power captured from the wind turbine is $a_0 = \frac{1}{3}$. This optimal induction factor gives rise to a power coefficient of $C_{P_0} = \frac{16}{27}$ and a thrust coefficient of $C_{T_0} = \frac{8}{9}$.

On a real turbine, C_P and C_T are typically modeled as functions of the tip-speed ratio λ and blade-pitch angle β which can be many-to-one mapping from (β, λ) to C_P and C_T [11]. We use $C_T(a)$ as an input in this paper which can be mapped into equivalent blade-pitch angle and tip-speed ratio contour. Choosing a specific (β, λ) pair then depends on other parameters like loads and operating conditions. There is no simple formula for this which is generically applicable to all turbines. However, for a given rotor, a tool like the standalone driver for AeroDyn v15 [12] can be used to compute the C_P and C_T as a function of β and λ.

B. Governing Equations

The actuator disk model [13], [14], [15] considered in this paper solves the 2D unsteady, incompressible Navier-Stokes equations assuming a linear drag force acting on the flow due to the turbine. The typical operating wind speeds for a wind turbine do not exceed Mach 0.1 at sea level and hence the assumption of incompressibility is justified. We assume that the freestream flow is orthogonal to the turbine rotor plane and that any disturbances in the freestream act solely to perturb the streamwise flow. We also assume that all velocities are non-dimensionalized by freestream velocity U_∞ [m/s], all spatial lengths are non-dimensionalized by the turbine diameter D, time t is non-dimensionalized by $T = 1s$ and pressure p is non-dimensionalized by ρU_∞^2. The dimensionless Navier-Stokes equation governing the evolution of the flow under the assumptions outlined above are given by:

$$\frac{\partial u}{\partial x} + \frac{\partial v}{\partial y} = 0$$

$$\frac{\partial u}{\partial t} + u\frac{\partial u}{\partial x} + v\frac{\partial u}{\partial y} = -\frac{\partial p}{\partial x} + \frac{1}{Re}\left(\frac{\partial^2 u}{\partial x^2} + \frac{\partial^2 u}{\partial y^2}\right) + f + f_D$$

$$\frac{\partial v}{\partial t} + u\frac{\partial v}{\partial x} + v\frac{\partial v}{\partial y} = -\frac{\partial p}{\partial y} + \frac{1}{Re}\left(\frac{\partial^2 v}{\partial x^2} + \frac{\partial^2 v}{\partial y^2}\right) + f$$

Here (u, v) denote the streamwise and spanwise velocity components and (x, y) denote the streamwise and spanwise coordinates. The Reynolds number, Re is defined as $Re := \frac{U_\infty D}{\nu}$ where ν [m^2/s] is the kinematic viscosity. f is the forcing due to the turbine and f_D is the disturbance forcing acting on the flow.

The forcing due to each turbine is a nonlinear function of space and the time-varying thrust coefficient, i.e. $f = f(x, y, C_T(t))$. For modeling purposes, this forcing is split into two components $f(x, y, C_T(t)) = f_T(x, y, C_{T_0}) + f_C(x, y, C_T(t))$. Here, f_T is the constant forcing due to the turbine operating at the a thrust coefficient of $C_{T_0} = \frac{8}{9}$ which corresponds to optimal axial induction factor of $a_0 = \frac{1}{3}$. The forcing profile for f_T is largest at the rotor hub and decreases in magnitude towards the blade tip. The forcing f_C is due to the variations in the axial induction. This term is modeled as a time-varying input $C_T(t)$ multiplied by a spatial profile. The input $C_T(t)$ can be mapped back to an equivalent axial induction factor $a(t)$. The spatial profile for f_C is smallest at rotor hub and increases in magnitude outwards towards the blade tip. The disturbance forcing f_D is a spatial sinusoid at approximately unit distance downstream from the inlet which spans the field in y-direction and acts to break the symmetry of the incoming flow. Additional details on the forcing functions can be found in the Appendix.

For the simulation of the actuator disk model, the equations are solved using a central differencing scheme [16]. The rectangular region with the turbine is divided into a grid with N_x points in the x-direction and N_y points in the y-direction. Each grid point is associated with a u and v velocity, thus the model has $2 \times N_x \times N_y$ states. For our particular example, the field is $L = 20$ units long in x-direction and $W = 5$ units wide in the y-direction. The turbine hub is located at $(x_0, y_0) = (5, 2.5)$. The spacing between the grid points is $\delta x = 0.1$ and $\delta y = 0.1$ with a time step of $\delta t = 0.01$. The resulting model has $20,502$ states. The boundary conditions of the model are set to:

$$u(x = 0, y, t) = u(x, y = 0, t) = u(x, y = W, t) = U_\infty$$
$$v(x = 0, y, t) = v(x, y = 0, t) = v(x, y = W, t) = 0$$

The Reynolds number for our simulation is set to 50. This small value of Re is not realistic for wind turbines where the appropriate Reynolds number is of the order of 10^6. However, for the purposes of this paper, we are restricting ourselves to a low Reynolds number to demonstrate the feasibility and possible insights that can be gained from full-information control of wake meandering.

C. Wake Meandering

Figure 1 shows an instantaneous pseudocolor plot of the streamwise (top subplot) and spanwise (bottom subplot) flow field in our simulation. For this simulation, the disturbance input is selected to be a uniformly distributed, zero-mean random signal with magnitude 0.3. The excitation input, C_T is a sum of sines at 1.1 and 1.23 rad/s superimposed with a uniformly distributed, zero-mean random noise of magnitude 0.1. The wake meandering as evidenced by the characteristic periodic lateral displacement of the wake behind the turbine can be clearly seen from the plot.

This meandering wake can cause many problems in a wind farm. Downstream turbines located in the path of such oscillating wakes experience fluctuating inflow conditions. The changing inflow conditions adversely affect the structural loads on downstream turbines. The unsteady loads can cause early onset of material and structural fatigue thereby adding to maintenance costs. Wake control can therefore give significant revenue boost by reducing the costs of operation. In the following sections, we obtain a reduced order model from the full-order actuator disk simulation and design a controller for the turbine wake meandering.

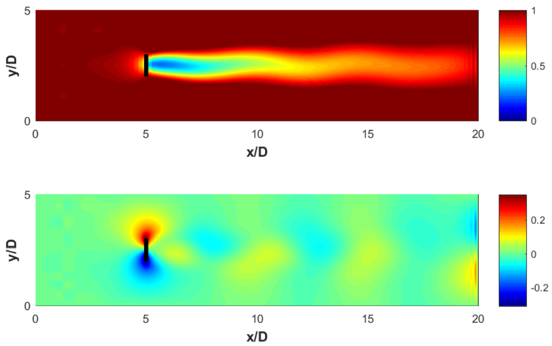

Fig. 1. Flow-field of the $20,502$ state simulation at $t = 45.0$. First subplot shows u and second subplot shows v. The vertical black line represents the location of the actuator disk.

III. MODEL REDUCTION

The actuator disk model obtained in the Section II-B has more than $20,000$ states, and as such is not suitable for control design. The nonlinearity of the model adds another complication as the extensive theory available for control of linear models can not be applied [17]. Therefore, we first construct a reduced order linear model that captures the dominant input-output behavior of the nonlinear model. There are several techniques available in literature for reducing the model order, such as balanced truncation [18], [19], proper orthogonal decomposition (POD) [20], [21], balanced POD [22], [23], [24], dynamic mode decomposition [25], [26], [27], and input-output reduced order models (IOROMs) [28], [29], [9]. A good overview of existing approaches can be found in [30].

For our problem we use the model reduction approach from [9] to obtain a two-input one-output linear model. The two inputs are the freestream disturbance and turbine thrust coefficient. The disturbance input is included in order to model its effect on the wake meandering. The thrust coefficient acts as the control input. The single output is the measurement of spanwise velocity v at $(x_M, y_M) = (13, 2.5)$. This output is convenient to observe the fluctuations in v due to wake meandering. The model is constructed at a single operating point defined by the non-dimensional freestream velocity U_∞ and optimal turbine input. In order to obtain the linear reduced order model, we excite the nonlinear system about the chosen operating point using the inputs and gather state, input and output snapshots from the simulation. One snapshot is gathered for every 20 steps of the nonlinear simulation giving an effective time step of $20\delta t = 0.2$. A lower-order projection basis for the states is obtained using proper orthogonal decomposition and then a linear model fit is obtained for the reduced state, input and output snapshots. The reduced order system matrices are given by:

$$\begin{bmatrix} F & G \\ H & D \end{bmatrix} = \begin{bmatrix} Q^T X_1 \\ Y_0 \end{bmatrix} \begin{bmatrix} Q^T X_0 \\ U_0 \end{bmatrix}^{\dagger} \tag{4}$$

where F, G, H, D are the matrices for the reduced order model, Q is the set of POD projection modes, and X_0, X_1, are the state snapshots and U_0 and Y_0 are respectively the input and output snapshots. $\dagger$ denotes the Moore-Penrose pseudoinverse of the matrix. Further details of the algorithm can be found in [9]. The approach can be extended to capture wider operating conditions using parameter-varying models [17] and gain-scheduled control.

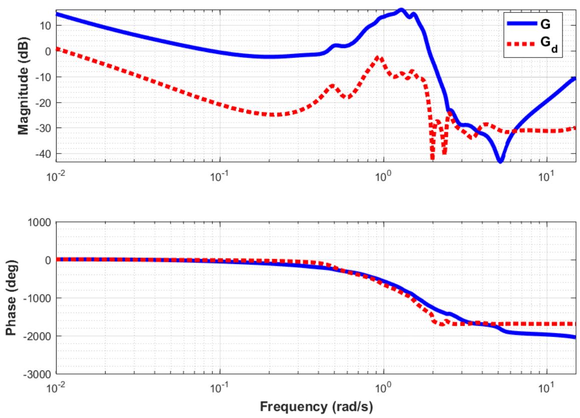

Fig. 2. Bode plots of the identified reduced order linear model.

A 34 state reduced order model is identified using this approach. The Bode plot of the identified reduced order model is given in Figure 2. In the figure, G corresponds to transfer function from C_T and G_d corresponds to transfer function from freestream disturbance to the measured output. The time step of 0.2 between snapshots gives a Nyquist frequency of $\omega_h = 15.71$ rad/s which is approximately 10 times the observed wake meandering frequency ($\approx 1 - 1.5$ rad/s). The total time of simulation was chosen to be 100 which sets the minimum identifiable frequency of $\omega_l = 0.06$ rad/s. The identification signal for input C_T was selected to be a chirp signal with frequency range $[\omega_l, \omega_h/2]$ rad/s and magnitude $1/9$ while a uniform random noise with magnitude 0.3 was selected as the disturbance input. Thus the identified model is valid between approximately 0.06 rad/s and 7.85 rad/s.

The validation results of the IOROM model for the same input as that described in Section II-C are given in Figure 3. The first subplot shows the output from the nonlinear system vs. the output obtained from IOROM. The green vertical line represents the time instant $t = 45.0$ for which the subsequent pseudocolor subplots are drawn. The pseudocolor plots in Figure 3 are obtained by lifting up the reduced order states to obtain approximations for the full-order nonlinear states. The reduced order model is able to adequately capture the nonlinear output as well as behavior of full-order system states as can be clearly seen by comparing the pseudocolor plots in Figure 3 to Figure 1.

IV. FULL-INFORMATION H_∞ CONTROLLER

The next step is to synthesize a controller using the reduced order model. Our initial designs could not reduce the wake meandering using the single measurement at (x_M, y_M). This section focuses on a full-information design to gain insight into additional measurements that are most beneficial. In particular, we investigate a full-information H_∞ controller that has access to all the states as well as the disturbance.

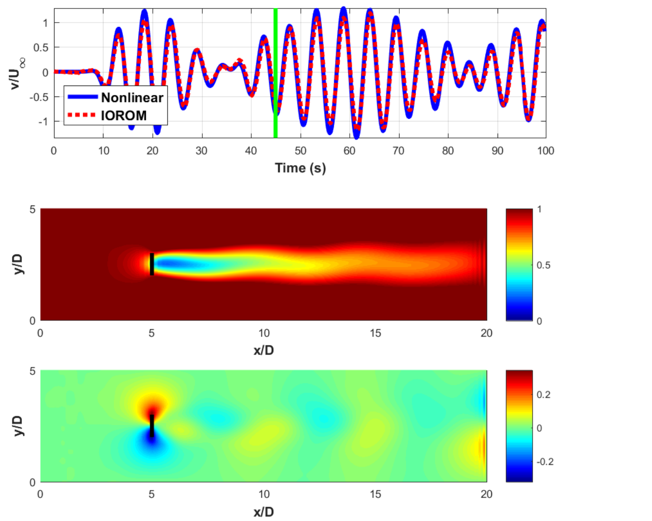

Fig. 3. IOROM validation results. First subplot compares the output of the reduced order system to that of full order simulation. Second and third subplots show the approximations to the full order states obtained from the reduced order states at $t = 45.0$

The solution for discrete-time full-information H_∞ controller is first described for a generic system. In particular, noting the slight abuse of the notation, consider a discrete-time linear system of the following form:

$$\begin{aligned} x_{k+1} &= Ax_k + B_1 u_k + B_2 d_k \\ e_k &= Cx_k + D_1 u_k + D_2 d_k \\ y_k &= \begin{bmatrix} I \\ 0 \end{bmatrix} x_k + \begin{bmatrix} 0 \\ I \end{bmatrix} d_k \end{aligned} \tag{5}$$

where $x_k \in \mathbb{R}^{n_x}$ is the state, $u_k \in \mathbb{R}^{n_u}$ is the control input, $d_k \in \mathbb{R}^{n_d}$ is the disturbance, $e_k \in \mathbb{R}^{n_e}$ is the error, and $y_k \in \mathbb{R}^{n_x+n_d}$ is the measurement. A, B_1, B_2, C, D_1 and D_2 are constant system matrices of appropriate dimensions. Note that the measurement vector includes the full state as well as the disturbance. Thus the controller has access to all possible information required to reduce the effect of the disturbance on the error.

A full-information H_∞ controller for the system in Eq. (5) is found by solving the following discrete-time algebraic Ricatti equation (DARE) [31]:

$$\begin{aligned} P =& A^T PA + C^T C \\ &- \begin{bmatrix} B_1^T PA + D_1^T C \\ B_2^T PA + D_2^T C \end{bmatrix}^T G(P)^{-1} \begin{bmatrix} B_1^T PA + D_1^T C \\ B_2^T PA + D_2^T C \end{bmatrix} \end{aligned} \tag{6}$$

where the matrix $G(P)$ is invertible and defined as

$$G(P) := \begin{bmatrix} D_1^T D_1 & D_1^T D_2 \\ D_2^T D_1 & D_2^T D_2 - I \end{bmatrix} + \begin{bmatrix} B_1^T \\ B_2^T \end{bmatrix} P \begin{bmatrix} B_1 & B_2 \end{bmatrix} \tag{7}$$

The controller is then given by the static feedback law $u_k = F_1 x_k + F_2 d_k$ where:

$$F_1 := -(D_1^T D_1 + B_1^T PB)^{-1}(B_1^T PA + D_1^T C), \tag{8}$$

$$F_2 := -(D_1^T D_1 + B_1^T PB)^{-1}(B_1^T PB_2 + D_1^T D_2) \tag{9}$$

Additional details can be found in [31].

This result is applied using the reduced order model for the actuator disk dynamics and hence $n_x = 34$. There is a single control input at the turbine ($n_u = 1$) and a single disturbance near the upstream boundary condition ($n_d = 1$). Finally, the error, i.e. the signal to be minimized, is a 2×1 vector containing the downstream lateral velocity and weighted input and thus $n_e = 2$. All these signals are as described in Section III. The next section discusses the performance of this full-information controller. In addition, the controller matrices are used to gain insights that can be used to identify the information that is most important for wake control.

V. RESULTS AND DISCUSSION

A full-information controller was designed using an augmented plant P obtained by augmenting the reduced order model with a weight $W = \frac{64}{27}\frac{(s+30)^3}{(s+40)^3}$ to penalize the control input at high frequencies.

$$P = \begin{bmatrix} W & 0 \\ G & G_d \end{bmatrix} \tag{10}$$

Note that the implementation of controller on the nonlinear model requires a projection of the full-order state down to the reduced order state using the projection modes. For the plant P, the controller can be written as $u_k = F_1 Q^T x_k^{full} + F_2 d_k + F_3 x_k^W$ where x_k^{full} is the full-order system state, x_k^W is the state of weight W, and Q^T contains the projection modes.

The full-order, nonlinear, actuator disk model was simulated with the controller and the results are shown in Figure 4. For

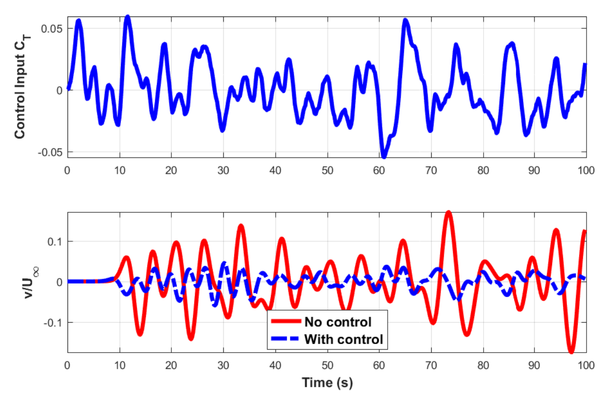

Fig. 4. Full-information controller results for the nonlinear model

this simulation, the actuator disk model was initialized at the base flow conditions and the input disturbance was designed to be a uniformly distributed, zero mean random noise signal of magnitude 0.3. The first subplot shows the control input C_T relative to the trim value of $C_{T_0} = \frac{8}{9}$. As the total thrust coefficient cannot exceed 1, the limiting positive value of control input is $1 - C_{T_0} \approx 0.11$. The required control effort never exceeds 0.06 so clearly the controller does not demand excessive control authority. The second subplot compares the output of the system without control (red line) with the controlled output (blue dashed line). It can be seen that the controller successfully suppresses the wake meandering.

The ideal, full-information controller obtained in Section IV can intuitively be understood to give the best possible control performance as there is no information hidden from the controller. While such a controller is not realistically implementable, the exercise provides several valuable insights. The first term $F_1 Q^T x_k^{full}$ of the control input can be understood as $K x_k^{full}$ where $K = F_1 Q^T$ is the control gain applied to full-order states. The distribution of values in K therefore informs about the states which are most important for control purposes. In other words, the states for which the control gain is high are most important to the full-information controller.

Figure 5 shows the pseudocolor plots of K for both streamwise and spanwise velocity components. There appear to be four locations which are important for u and two locations which are most important for v. These points of importance, i.e. large magnitude gains, correspond to the areas of sharp red or blue color downstream of the turbine. We think that the four highlighted gains in the streamwise direction might be the controller attempting to act on the vorticity of the flow. However, further investigations are underway.

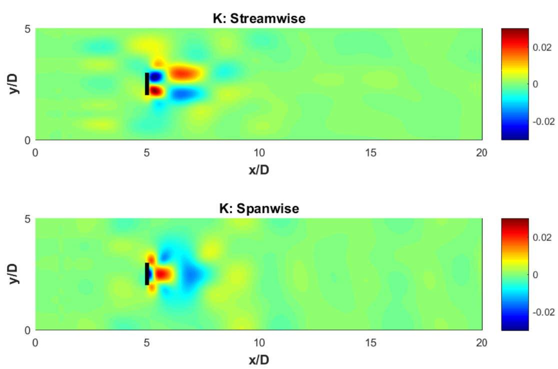

Fig. 5. Controller Insight from distribution of control gain K

We hypothesize that using only six measurements at locations corresponding to high gain as inputs for an output measurement based controller we might be able to recover most of the full-information control performance. Another approach would be try to estimate these states from measurements at other, perhaps more feasible locations and use those estimates for an observer based control design.

To test our hypothesis, we made the disturbance gain $F_2 = 0$ to neglect the disturbance feedback and then gradually zeroed out the entries in the gain matrix[1] starting from the smallest to the largest in magnitude. As K is gradually emptied, the gains at those six locations are preserved the longest (being largest in magnitude) while the smaller gains are made zero. Using these gain matrices, the simulation was rerun and the variance in the measured controlled output was calculated. Figure 6 shows the semi-log plot of variance of controlled output (normalized with respect to the open loop variance) vs. the log of percentage of non-zero entries in K. The results are encouraging and it can be seen that with only $\approx 15\%$ non-zero entries in K, the variance in output is better than that obtained using the full gain matrix[2]. When $\approx 100\%$ of the entries of K are zero, the system is essentially running with no control and the normalized closed loop variance approaches 1. More formal sparsity-promoting techniques [32] will be investigated in the future for obtaining a sparse K.

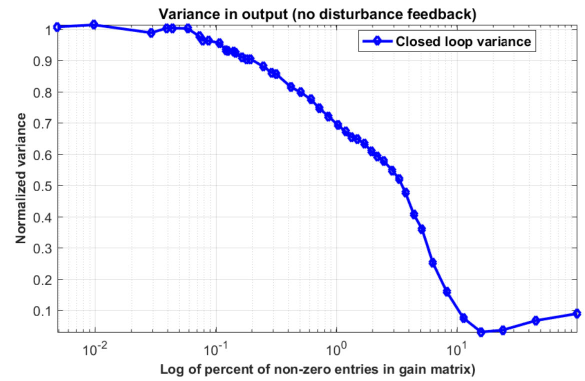

Fig. 6. Variance in measured output (normalized w.r.t. open-loop variance) as the entries of gain matrix K are zeroed out

VI. CONCLUSIONS

This paper considers the control of wake meandering behind a turbine modeled with a simplified, nonlinear 2D actuator disk model. A linear reduced order model is constructed from input-output data to approximate the full-order nonlinear simulation. This reduced order model is then used to design a full-information controller which is successfully validated in the nonlinear simulation. The control gains of the full-information controller are used to identify the information most useful for control. This approach can also be used for analyzing a full-information controller for a wind farm model in Simulator fOr Wind Farm Applications (SOWFA). The insights gained from high-fidelity models like SOWFA can be valuable in deciding measurement locations and designing controllers for actual wind farms, which also forms a direction for further future work.

APPENDIX

A. Turbine Forcing

As the hub of the turbine is placed at (x_0, y_0), the rotor plane lies within $(y_0 - \frac{1}{2}) \leq y \leq (y_0 + \frac{1}{2})$. The forcing terms introduced by the turbines are defined as:

$$\begin{aligned} f_T(x, y, C_{T_0}) &= 0.7 C_{T_0} C_{\theta_x} C_{\theta_y} (1 - |\Delta_x|)(1 - |\Delta_y|)^{0.7} \\ f_C(x, y, C_T(t)) &= C_T(t) \text{sign}(\Delta_y)(1 - |\Delta_x|)|\Delta_y|^{0.7} \\ &\quad \text{for } (x_0 - 2\delta x) \leq x \leq (x_0 + 2\delta x) \\ &\quad \text{and } (y_0 - \tfrac{1}{2} - 2\delta y) \leq y \leq (y_0 + \tfrac{1}{2} + 2\delta y). \end{aligned}$$

For all other values of x and y, $f_T = 0$ and $f_C = 0$. Here $\Delta_x = (x - x_0)$ is the x-direction displacement from the hub center, δx is the x-spacing between grid-points, and

[1] It is important to note that, in general, modifying the control gain matrix can cause the closed loop system to go unstable.

[2] This increase in performance is because we are optimizing with respect to the H_∞ norm but then doing the performance evaluation (Figure 6) with respect to output variance.

$C_{\theta_x} = \cos\frac{\pi}{2}\frac{\Delta x}{2\delta x}$ works to smooth the transition from unforced to forced region in the flow field. Δ_y, δy and C_{θ_y} are defined analogously in terms of y. C_{T_0} is the thrust coefficient of the turbine operating the optimum axial induction factor of $a = \frac{1}{3}$, and $C_T(t)$ is the variation of thrust coefficient about this optimum value.

B. Disturbance Forcing

The disturbance forcing is intended to break the spatial symmetry of the free stream. The forcing acts at approximately $1D$ downstream of the flow field inlet. The disturbance forcing can be computed as per the below pseudocode:

```
Initialize f_D = zeros(N_x, N_y)
for i = 1 to N_y − 4
    for j = 1 to 4
        for k = 1 to 4
            x = k + 9
            y = N_X * (i + j − 1)
            C_x = 0.25 * (1 + cos((k − 2.5) π/2))
            C_y = 0.25 * (1 + cos((j − 2.5) π/2))
            f_D(x, y) = f_D(x, y) + g(i) C_x C_y
        end loop of k
    end loop of j
end loop of i
```

where g is given by:

$$g(y) = \sum_{i=1}^{8} sin(2\pi(i\frac{y}{N_y} + \texttt{rand})) \tag{11}$$

Here `rand` is a random number between 0 and 1.

ACKNOWLEDGMENT

The authors would like to acknowledge useful comments from Jen Annoni. This work was supported by the National Science Foundation under Grant No. NSF-CMMI-1254129 entitled CAREER: Probabilistic Tools for High Reliability Monitoring and Control of Wind Farms. The work was also supported by the MnDrive project entitled Sustainable Energy Systems: Control Systems and Sensors to Link Rural Renewables and Demand for Sustainable Industrial Energy in Food Processing Systems

REFERENCES

[1] B. Sanderse, "Aerodynamics of wind turbine wakes - literature review," tech. rep., Energy research Centre of the Netherlands, 2009.

[2] D. Medici and H. Alfredsson, "Wind turbine near wakes and comparisons to the wake behind a disc," in *43rd AIAA Aerospace Sciences Meeting and Exhibit*, p. 595, 2005.

[3] D. Medici and P. H. Alfredsson, "Measurements behind model wind turbines: further evidence of wake meandering," *Wind Energy*, vol. 11, no. 2, pp. 211–217, 2008.

[4] G. España, S. Aubrun, S. Loyer, and P. Devinant, "Spatial study of the wake meandering using modelled wind turbines in a wind tunnel," *Wind Energy*, vol. 14, no. 7, pp. 923–937, 2011.

[5] G. C. Larsen, H. A. Madsen, K. Thomsen, and T. J. Larsen, "Wake meandering: a pragmatic approach," *Wind Energy*, vol. 11, no. 4, pp. 377–395, 2008.

[6] K. E. Johnson and N. Thomas, "Wind farm control: addressing the aerodynamic interaction among wind turbines," in *2009 American Control Conference*, pp. 2104–2109, IEEE, 2009.

[7] S. Aubrun, G. España, S. Loyer, P. Hayden, and P. Hancock, *Is the Actuator Disc Concept Sufficient to Model the Far-Wake of a Wind Turbine?*, pp. 227–230. Berlin, Heidelberg: Springer Berlin Heidelberg, 2012.

[8] Y.-T. Wu and F. Porté-Agel, "Large-eddy simulation of wind-turbine wakes: Evaluation of turbine parametrisations," *Boundary-Layer Meteorology*, vol. 138, no. 3, pp. 345–366, 2011.

[9] J. Annoni and P. Seiler, "A method to construct reduced-order parameter-varying models," *International Journal of Robust and Nonlinear Control*, vol. 27, no. 4, pp. 582–597, 2017.

[10] T. Burton, D. Sharpe, N. Jenkins, and E. Bossanyi, *Wind energy handbook*. John Wiley & Sons, 2001.

[11] J. Aho, A. Buckspan, J. Laks, P. Fleming, Y. Jeong, F. Dunne, M. Churchfield, L. Pao, and K. Johnson, "A tutorial of wind turbine control for supporting grid frequency through active power control," in *American Control Conference (ACC), 2012*, pp. 3120–3131, IEEE, 2012.

[12] "NWTC Information Portal (AeroDyn)." https://nwtc.nrel.gov/AeroDyn. Last modified 27-July-2016; Accessed 13-February-2017.

[13] J. N. Sørensen and A. Myken, "Unsteady actuator disc model for horizontal axis wind turbines," *Journal of Wind Engineering and Industrial Aerodynamics*, vol. 39, no. 1-3, pp. 139–149, 1992.

[14] J. N. Sørensen and C. W. Kock, "A model for unsteady rotor aerodynamics," *Journal of wind engineering and industrial aerodynamics*, vol. 58, no. 3, pp. 259–275, 1995.

[15] J. Annoni, J. Nichols, and P. Seiler, "Wind farm modeling and control using dynamic mode decomposition," in *34th Wind Energy Symposium*, vol. 2201, 2016.

[16] O. Zikanov, *Essential computational fluid dynamics*. John Wiley & Sons, 2010.

[17] S. Skogestad and I. Postlethwaite, *Multivariable feedback control: analysis and design*, vol. 2. Wiley New York, 2007.

[18] B. C. Moore, "Principal component analysis in linear systems: Controllability, observability, and model reduction," *IEEE Transactions on Automatic Control*, vol. 26, no. 1, pp. 17–32, 1981.

[19] L. Pernebo and L. M. Silverman, "Model reduction via balanced state space representations," *IEEE Transactions on Automatic Control*, vol. 27, no. 2, pp. 382–387, 1982.

[20] G. Berkooz, P. Holmes, and J. L. Lumley, "The proper orthogonal decomposition in the analysis of turbulent flows," *Annual Review of Fluid Mechanics*, vol. 25, no. 1, pp. 539–575, 1993.

[21] P. Holmes, J. L. Lumley, and G. Berkooz, *Turbulence, coherent structures, dynamical systems and symmetry*. Cambridge University Press, 1998.

[22] K. Willcox and J. Peraire, "Balanced model reduction via the proper orthogonal decomposition," *AIAA Journal*, vol. 40, no. 11, pp. 2323–2330, 2002.

[23] C. Rowley, "Model reduction for fluids, using balanced proper orthogonal decomposition," *International Journal of Bifurcation and Chaos*, vol. 15, no. 03, pp. 997–1013, 2005.

[24] S. Lall, J. E. Marsden, and S. Glavaški, "A subspace approach to balanced truncation for model reduction of nonlinear control systems," *International Journal of Robust and Nonlinear Control*, vol. 12, no. 6, pp. 519–535, 2002.

[25] P. Schmid, "Dynamic mode decomposition of numerical and experimental data," *Journal of Fluid Mechanics*, vol. 656, pp. 5–28, 2010.

[26] J. L. Proctor, S. L. Brunton, and J. N. Kutz, "Dynamic mode decomposition with control," *SIAM Journal on Applied Dynamical Systems*, vol. 15, no. 1, pp. 142–161, 2016.

[27] I. Mezič, "Spectral properties of dynamical systems, model reduction and decompositions," *Nonlinear Dynamics*, vol. 41, no. 1-3, pp. 309–325, 2005.

[28] T. Lieu, C. Farhat, and M. Lesoinne, "Reduced-order fluid/structure modeling of a complete aircraft configuration," *Computer Methods in Applied Mechanics and Engineering*, vol. 195, no. 41, pp. 5730–5742, 2006.

[29] B. P. Danowsky, P. M. Thompson, C. Farhat, T. Lieu, C. Harris, and J. Lechniak, "Incorporation of feedback control into a high-fidelity aeroservoelastic fighter aircraft model," *Journal of Aircraft*, vol. 47, no. 4, pp. 1274–1282, 2010.

[30] A. C. Antoulas, *Approximation of large-scale dynamical systems*, vol. 6. SIAM, 2005.

[31] A. A. Stoorvogel, *The H_∞ Control Problem: A State Space Approach*. Prentice Hall, 1992.

[32] F. Lin, M. Fardad, and M. R. Jovanović, "Design of optimal sparse feedback gains via the alternating direction method of multipliers," *IEEE Transactions on Automatic Control*, vol. 58, no. 9, pp. 2426–2431, 2013.